In-air sintering of copper nanoparticle paste with pressure-assistance for die attachment in high power electronics

Zhang, Boyao; Damian, Andrei; Zijl, Jurrian; van Zeijl, Henk; Zhang, Yu; Fan, Jiajie; Zhang, Guoqi

DOI
10.1007/s10854-020-05196-4

Publication date
2021

Document Version
Final published version

Published in
Journal of Materials Science: Materials in Electronics

J Mater Sci: Mater Electron

In-air sintering of copper nanoparticle paste with pressure-assistance for die attachment in high power electronics

Boyao Zhang[1], Andrei Damian[2], Jurrian Zijl[3], Henk van Zeijl[1], Yu Zhang[4,*], Jiajie Fan[5], and Guoqi Zhang[1,*]

[1] *Department of Microelectronics, Faculty of Electronics, Mathematics and Information, Delft University of Technology, 2628 CT Delft, South Holland, The Netherlands*
[2] *NXP Semiconductors, 6534 AE Nijmegen, Gelderland, The Netherlands*
[3] *Besi Netherlands B.V, 6921 RW Duiven, Gelderland, The Netherlands*
[4] *State Key Laboratory of Precision Electronic Manufacturing Technology and Equipment, Guangdong University of Technology, Guangzhou 510006, China*
[5] *Center for Shanghai Silicon Carbide Power Devices Engineering & Technology Research, Academy for Engineering & Technology, Fudan University, Shanghai 200433, China*

Received: 19 October 2020
Accepted: 24 December 2020

ABSTRACT

There is a high demand for the implementation of metallic nanoparticle (NP) sintering technology for die attach in high-power electronics. The performance of this technology is superior to that of the technology involving the use of lead-free solders. Although Cu NP paste is potentially a low-cost material, it faces the challenge of oxidation during sintering. This may result in a significant deterioration of the mechanical, thermal, and electrical properties. Therefore, there are limited studies on the in-air sintering of Cu NP pastes. The present study demonstrated the in-air pressure-assisted low-temperature sintering of a commercial Cu NP paste. Furthermore, the sintering was performed without using a protective atmosphere, unlike that in most of the previously reported investigations. The sintering behavior was investigated at three levels of temperatures (200–240 °C) and five levels of pressures (5–25 MPa). The joints that were sintered at high temperatures and pressures exhibited condensed microstructures and high bonding strengths. High sintering temperatures accelerated the diffusion between Cu NPs, while high sintering pressure facilitated the removal of evaporated organic compounds and the air between NPs. This not only facilitated sintering but also prevented the oxidation of Cu. The optimal sintering conditions promoted the formation of 3D connections between the Cu NPs, thereby increasing the shear strength of the sample. The samples that were sintered at 240 °C and 10 MPa experiences the highest increase in the shear strength, furthermore, the microstructures were optimized under this condition.

Address correspondence to E-mail: zhangyu@gdut.edu.cn; g.q.zhang@tudelft.nl

https://doi.org/10.1007/s10854-020-05196-4
Published online: 12 January 2021

The shear strength of 28.1 ± 8.47 MPa was achieved under this condition, which satisfied the requirements for die attach in high power electronics applications, moreover, the sintering process was moderate and cost-effective. Therefore, the optimal sintering temperature and pressure for the in-air sintering of the Cu NP paste was concluded to be 240 °C and 10 MPa, respectively. The results indicated that in-air sintering with pressure assistance can be applied for die attach in the high-power electronics.

1 Introduction

The requirement for miniaturization and integration drives the advancements in the power electronics industry [1–3]. High power electronics are often applied in harsh environments, such as aerospace, energy production, and automotive applications. The working temperatures of power electronics devices that are based on wide-bandgap semiconductors, such as gallium nitride (GaN) and silicon carbide (SiC), often exceed 200 °C and, occasionally reach 350 °C. However, the presently available power electronics components and packaging technologies cannot satisfy such high-temperature requirements. The conventional Pb-free die-attach materials, such as SnAgCu (SAC) alloys, exhibit a reflow temperature of 220–260 °C [4, 5]. The operating temperature of AuSn is higher than that of SAC alloys, however, the large-scale production of AuSn is expensive. Therefore, the novel die-attach materials must overcome the challenges during both packaging processes and applications, by achieving a compatible process temperature and high operating temperatures, Furthermore, they must possess excellent thermal and electrical properties [6].

Metallic nanoparticles (NPs) are one of the most promising candidates for die-attach or interconnection in high power electronics [7]. The investigation into the size effect of metallic NPs revealed that metallic NPs can be sintered to form bulk materials at temperatures below 300 °C, which is compatible with the current process flow [8]. Consequently, the operating temperature of these materials can be increased beyond that of SAC solders. Furthermore, the growth of intermetallic compounds and Kirkendall voids can be avoided, via the use of one-type sintered materials [9, 10]. These advantages have encouraged the recent utilization of Ag NP paste as a die-attach material in power electronics applications [11–13]. The sintering parameters and materials were tuned to increase the mechanical strength of the sintered joints [14–16]. There have also been studies on the sintering mechanisms of Ag pastes [17–19]. However, Ag NP paste is susceptible to electromigration, and this is a concerning issue in high-current flow applications. There are reports on the migration-related issues that are experienced by sintered silver joints at high operation temperatures [16, 20, 21]. The thermo-electrical properties of Cu are similar to those of Ag, however, the resistance of Cu to electromigration is higher than that of Ag. Therefore, Cu NP paste has become an emerging die-attach material in high power electronics. The experimental sintering behavior of Cu NPs indicated that these particles can be sintered below 300 °C [22]. The properties of the sintered Cu NPs are similar to those of bulk Cu. Therefore, it can withstand a higher operating temperature than that of SAC alloy.

The easy oxidation of Cu NPs in air is a barrier to sintering. A reductive or protective sintering atmosphere is necessary for sintering of Cu NP paste to prevent the oxidation of the Cu NPs. Recently, there have been multiple reports on the fabrication Cu NP paste. The aim of these investigations was to analyze and subsequently optimize the performance of the sintered Cu NP paste as a die-attach material. Sintering has been conducted under various atmospheres, including formic acid gas [23], 5% H_2 + 95% N_2 [24, 25], and Ar + H_2 [26], to reduce copper oxides and prevent the additional oxidation of the Cu NPs, with pressure assistance. A high shear strength of 51.7 MPa was achieved using pressure-assisted sintering with reductive treatments [23]. Here, the samples were treated using formic acid treatment under an external pressure of 10 MPa for 10 min at 260 °C to achieve a high adhesion strength. The experiment included a dedicated wet chemical treatment and a prolonged sintering process. However, the use of processing gas and complex wet

chemical treatments, as in industrial applications, is time consuming and expensive.

The external pressure, in addition to the atmosphere, is another critical parameter. Although pressureless sintering offers the advantage of process simplicity, it requires strict process conditions and complex pre-treatments. A 100% H_2 atmosphere is required during pressureless sintering to achieve high shear strengths [27, 28]. Furthermore, the positive effect of reductive additives and surface modifications on the shear strength, without the application of external sintering pressure during the sintering, has been demonstrated [29]. Pressureless sintering has also been performed under 5% H_2 + 95% N_2 or inert gas atmospheres [30, 31]. However, the shear strength of the Cu NP joints that are sintered in the absence of external pressure is generally limited to less than 10 MPa. This may satisfy the requirements of some applications, that do not require high shear strengths. However, the application of external pressure to increase the shear strength of the sintered joints is necessary for applications such as die attachment in power electronics. The shear strength of the sintered joints can be increased to 20 MPa via pressure-assisted sintering in air using a mixture of various particle sizes [32]. A sintering time of between 20 min and 1 h, or even longer is required to achieve a high shear strength, and prolonged sintering decreases the production throughput. The requirement of strict sintering atmospheres and complex material treatments increase the cost and complexity of the manufacturing process. Consequently, the application of pressure-assisted sintering under ambient atmospheres, without any complexities of process conditions, to achieve high-quality sintered Cu NP joints, has becomes an essential topic of research.

In-air pressure-assisted sintering was proposed and performed using a commercialized Cu NP paste in the present study. The sintering behaviors and the microstructures of the sintered Cu NP joints at various pressures and temperatures were analyzed. The mechanical properties of the sintered Cu NP joints were investigated using shear tests. The corresponding fracture modes and microstructures of the fracture surfaces were characterized by using scanning electron microscopy/focused ion beam (SEM/FIB). Finally, a possible pressure-assisted sintering mechanism of the Cu NP paste in air was proposed.

2 Material characterization and methods

2.1 Cu NP paste characterization

The Cu NP paste (43.6 mg) was subjected to thermogravimetric analysis (TGA, STA 449, Netzsch-Gerätebau GmbH, Selb, Germany) from room temperature (25 °C) to 500 °C with a ramping rate of 10 °C/min, under Ar and air atmospheres. The paste exhibited mass loss with the increase in the temperature under the selected atmospheres. The composition of and the phase changes in the Cu NP paste were investigated via elevated-temperature X-ray diffraction (XRD, D5005, Bruker Corporation, Massachusetts, USA) with a Cu Kα (λ = 1.54 Å) X-ray source, and the theta/theta scan method was applied. To analyze the material changes at various temperatures, the instrument was equipped with a Pt heating strip to increase the sample temperature. A thin layer of the Cu NP paste was dispensed on a 10 mm × 10 mm Si substrate. The Cu NP paste on the Si substrate was initially dried in an N_2 oven at 80 °C for 30 min. Subsequently, it was placed on the Pt heating strip of the XRD instrument. The temperature of the sample was monitored using a thermocouple. The sample was heated from 25 to 300 °C, at intervals of 50 °C. The XRD scan was conducted after the sample was heated and soaked at each stabilized temperature.

2.2 Cu NP paste sintering and joint characterization

A 0.5 mm-thick Si wafer, that was sputtered with a metal stacking layer comprising 500 nm-thick Al, 200 nm-thick Ni, and 300 nm-thick Cu (Sigma deposition system, SPTS Technologies Ltd., Newport, Wales, UK), was used in this experiment. A Cu seed layer was applied to increase the adhesion between the Si wafer to the Cu NP paste. The prepared Si wafer with metal layers was sawn into 2 mm × 2 mm dies for pressure-assisted sintering. Direct-bonded copper (DBC) boards with a Cu plating layer were used as substrates. The paste was dispensed from a syringe on the DBC in an X shaped pattern. Dies were placed on top of the dispensed pattern and paste was squeezed out to fill the area underneath. The bond line thickness was measured to be 10 µm. The drying step was conducted to remove the low-organic solution and moisture from the paste. The drying step

was performed at 80 °C for 30 min under an N_2 atmosphere. Pressure-assisted sintering was conducted in air using industrial equipment that was supported by Besi Netherlands B.V., Duiven, The Netherlands (Fig. 1b). Figure 1a shows a schematic of the cross-section of the pressure-assisted sintering setup. The top and bottom press plates (plates 1 and 2 in Fig. 1a) were initially preheated at the recommended sintering temperature. Subsequently, the DBC substrates with the attached Si dies were placed between the two plates. These plates exerted the axial force and acted as the temperature source, simultaneously. The temperature, pressure, and holding time were precisely controlled using the equipment. The holding time during the sintering was maintained at 3 min for all the sintering experiments. Furthermore, no protective gases were used during sintering. The sintering behavior of the Cu NP paste was investigated under various sintering temperatures and pressures. One batch of samples was sintered and characterized under each sintering condition. Each batch comprised 10–15 Si dies on the DBC substrates.

The shear strengths of the samples after sintering were measured using a ball shear/die-shear tester (4000 Bondtester, Nordson Dage, Aylesbury, UK), under various sintering conditions. The optical images of the fractured surfaces of the sintered Cu joints were obtained via digital microscopy (AM3113T, Dino-Lite Digital Microscope, AnMo Electronics Corporation, Hsinchu, Taiwan). The microstructures of the fractured surfaces of the sintered Cu joints were characterized using a scanning electron microscope (NovaNano, FEI Company (Thermo Fisher Scientific), Oregon, USA). The cross-sections of the sintered Cu joints were analyzed using a FIB and energy-dispersive X-ray spectroscopy [EDS; Helios G3-CX, FEI Company (Thermo Fisher Scientific), Oregon, USA].

3 Results and discussion

3.1 Sintering temperature determination

The Cu NP paste is comprised of Cu NPs and multiple types of organic additives. Therefore, TGA and the in situ XRD measurements were performed to determine the appropriate sintering temperature range. Figure 2 shows the TGA results of the mass loss and thermal behavior of the Cu NP paste. The mass loss from 50 to 400 °C, in three stages, under an Ar atmosphere, was 12.2%. The mass loss in the first stage from 50 to 110 °C was 0.5%, which was attributed possibly to the presence of moisture and low-evaporation-temperature organic compounds. A rapid mass loss of 8.9% was observed in the second stage from 110 to 182.9 °C. The occurrence of the maximum mass loss in this stage indicated that the evaporation or decomposition of most of the solvents. A slow mass loss of 2.8% was observed in the third stage, from 182.9 to 400 °C. The diverse types of organic additives in the conductive paste exhibited various evaporation and decomposition temperatures.

In the curves of the TGA results under compressed air denoted the occurrence of mass loss in four stages. A slow mass loss was observed in the first stage from 50 to 110 °C, similar to the observations in the first stage under Ar. A rapid mass loss of 9.1% was

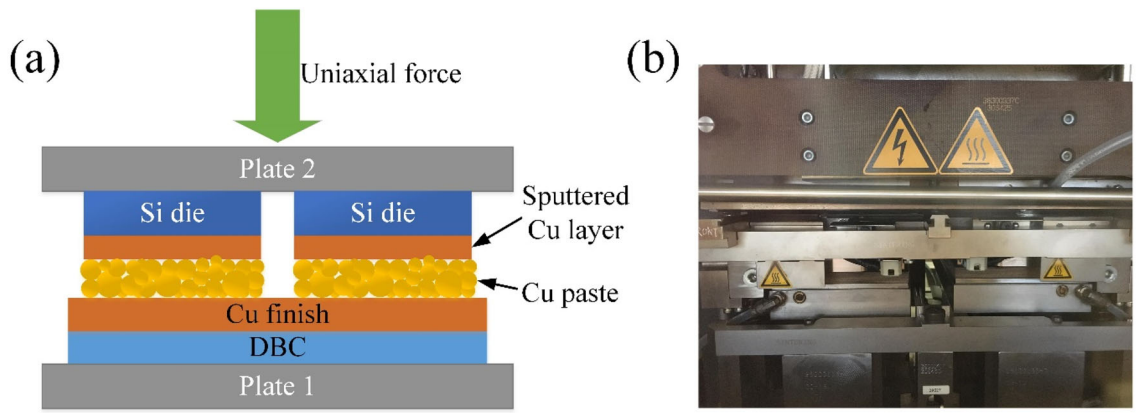

Fig. 1 **a** Schematic cross-section of the pressure-assisted sintering setup. **b** Pressure-assisted sintering equipment

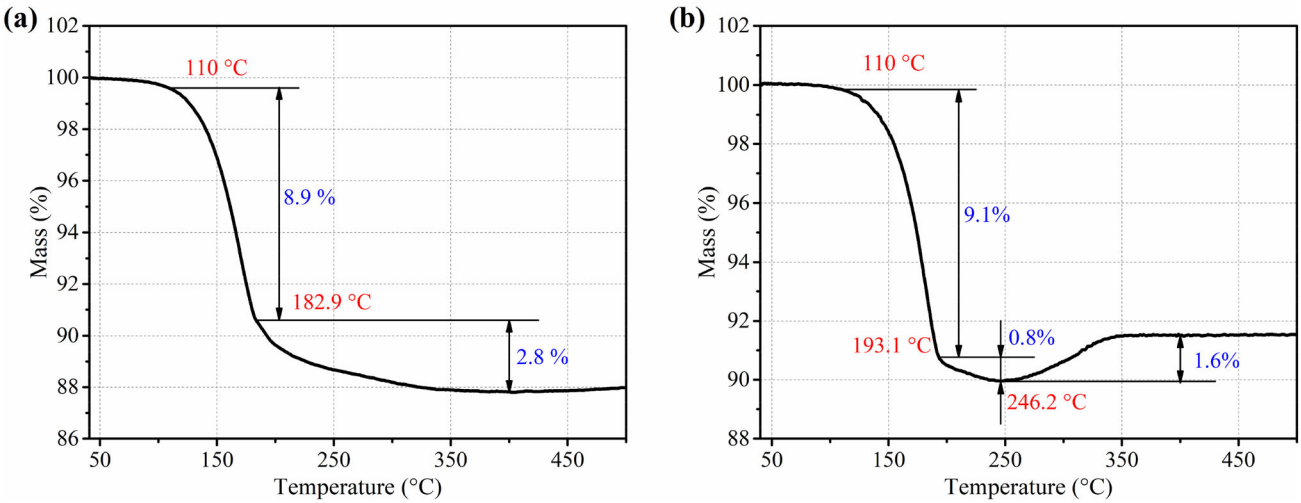

Fig. 2 TGA results of the Cu NP paste in **a** Ar and **b** compressed air

observed in the second stage of the process from 110 to 193.1 °C. The highest mass loss occurred during this stage of the process owing to the evaporation and decomposition of multiple organic compounds. The upper limit of the temperature in the second stage under compressed air (193.1 °C) was higher than that in the second stage under Ar (182.9 °C). This variation was attributed to the difference in the atmospheres. A slow mass loss of 0.8% was observed in the third stage from 193.1 to 246.2 °C. A 1.6% increase in the mass was observed in the final stage from 246.2 to 400 °C. The measurement under Ar indicated that the sample underwent additional mass loss above 246.2 °C. The Cu NPs were highly susceptible to oxidation above 193.1 °C, owing to the low solvent protection. Therefore, the mass variation in the final two stages probably comprised the increase in the mass due to the oxidation of Cu as well as the decrease in the mass owing to the evaporation of organic compounds. The effect of the organic evaporation was stronger than that of the oxidation in the third stage, thereby resulting in mass loss. The increase in the mass owing to oxidation was higher than the decrease in the mass owing to the evaporation in the final stage. Consequently, there was an increase in the mass above 246.2 °C. The results indicated that the Cu NP paste possessed low organic residuals and underwent moderate oxidation between 193.1 and 246.2 °C. Therefore, the appropriate sintering temperature in air was determined to be between 193.1 and 246.2 °C.

Elevated XRD analysis was performed in air to elucidate the material composition and structural changes during sintering. Figure 3 shows the XRD patterns of Cu NP paste at various high temperatures. The presence of three strong Cu peaks in the XRD pattern from room temperature to 150 °C indicated that Cu NPs were resistant to oxidation until relatively high temperatures. When the temperature was 200 °C, a weak Cu_2O (111) peak appeared at $2\theta = 36.9°$ in the XRD pattern. However, the intensities of the Cu_2O (111) and (220) peaks at 200 °C were negligible. These observations indicated the initiation

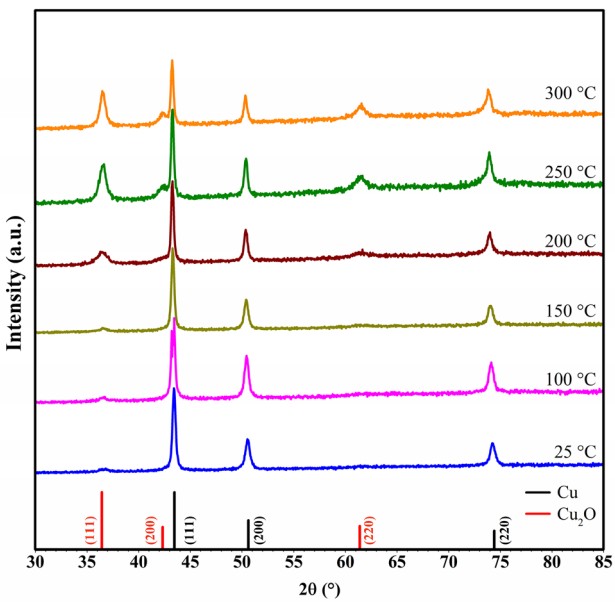

Fig. 3 X-ray diffraction scans of the Cu NPs paste at elevated temperatures in air

of oxidation, and the Cu NPs were slightly oxidized. The oxidation resistance of the Cu NPs in the paste before 200 °C was probably owing to the presence of an organic protection layer till 193.1 °C, as indicated by the TGA measurements (Fig. 2b). The Cu NPs remained exposed to air without organic protection at an elevated temperature of 250 °C. There was a significant increase in the strength of the Cu_2O (111) peak and the other Cu_2O peaks such as Cu_2O (200) and Cu_2O (220) appeared in the XRD pattern. The continuous growth of the Cu_2O peaks from 250 to 300 °C indicated the further oxidation of the Cu NPs. The results of the XRD analysis were correlated with those of TGA under the compressed air (Fig. 2b). It was inferred that the oxidation of the Cu NPs above 250 °C was the primary contributor to the increase in the mass above 246.2 °C. The results revealed that the Cu NP paste was resistant to oxidation below 200 °C in air, and it was partially oxidized between 200 and 250 °C.

The results of TGA measurements under Ar and compressed air and elevated-temperature XRD analysis (in air) indicated that most of the organic additives in the Cu NP paste were removed above 193.1 °C. Furthermore, the oxidation level of the Cu NP paste in air remained relatively low until 250 °C. Therefore, the appropriate in-air sintering temperature for the Cu NP paste in the present study was determined to be between 200 and 250 °C.

3.2 Optimization of the sintering parameters and characterization of the sintering joint

Three sintering temperatures, i.e., 200 °C, 220 °C to 240 °C, and five levels of external pressure, i.e., 5, 10, 15, 20, and 25 MPa, were selected for the experiment based on the results of TGA and XRD. Each batch was naturally cooled down to room temperature after 3 min of sintering. The sintered Cu NP joints were subjected to the shear strength test to evaluate the mechanical properties. Figure 4 shows the shear strength of the sintered Cu NP joints that were prepared at various sintering temperatures and pressures.

The samples that were sintered at 200 °C under 5 MPa presented the lowest shear strength of 0.29 MPa. There was a slight increase in the shear strength to 4.46 MPa with an increase in the sintering pressure to 25 MPa. The samples that were sintered

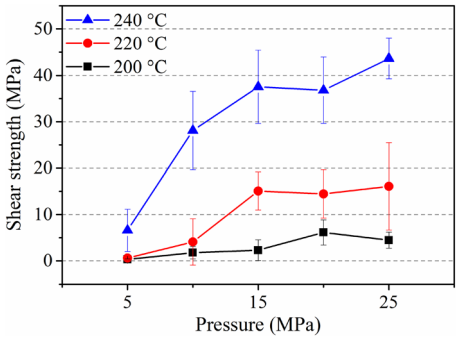

Fig. 4 Shear strength of sintered Cu NP joints at various temperatures and pressures

at 220 °C under 5 MPa presented a low shear strength of 0.61 MPa. There was a significant increase in the shear strength to 15.09 MPa with the increase in the pressure to 15 MPa, however, an additional increase in the external pressure at 220 °C did not induce any further increase in the shear strength. The samples that were sintered at 240 °C under 5 MPa presented a shear strength of 6.59 MPa. The shear strength increased more than four times, from 6.59 to 28.1 MPa, which was the highest observed increase, with the increase in the external pressure from 5 to 10 MPa. The shear strength continued to increase with the increase in the external pressure from 10 to 25 MPa. However, the rate of increase in the shear strength from 10 to 25 MPa was significantly lower than the rate of increase in the shear strength from 5 to 10 MPa. The highest shear strength of 41.63 ± 4.35 MPa was achieved at 240 °C under 25 MPa. The samples that were sintered at 240 °C under 10 MPa presented a shear strength of 28.1 ± 8.47 MPa, which satisfied the requirements for die attach in power electronics applications. Furthermore, there is a risk of sample damage under excessively high sintering pressures. Therefore, the optimal sintering temperature and pressure were determined to be 240 °C and, 10 MPa, respectively.

The surface morphologies of the macrofractures and microfracture were analyzed after the shear strength test. Thus, the fracture mode of the Cu NP joints under various sintering conditions was determined. The optical images of the shear surfaces and the fracture modes of representative samples under each sintering condition are presented in Fig. 5a. Two types of fracture modes, adhesive, and cohesive were observed. The cohesive fracture occurred inside the Cu joints (Fig. 5b). Only the Cu NPs were observed

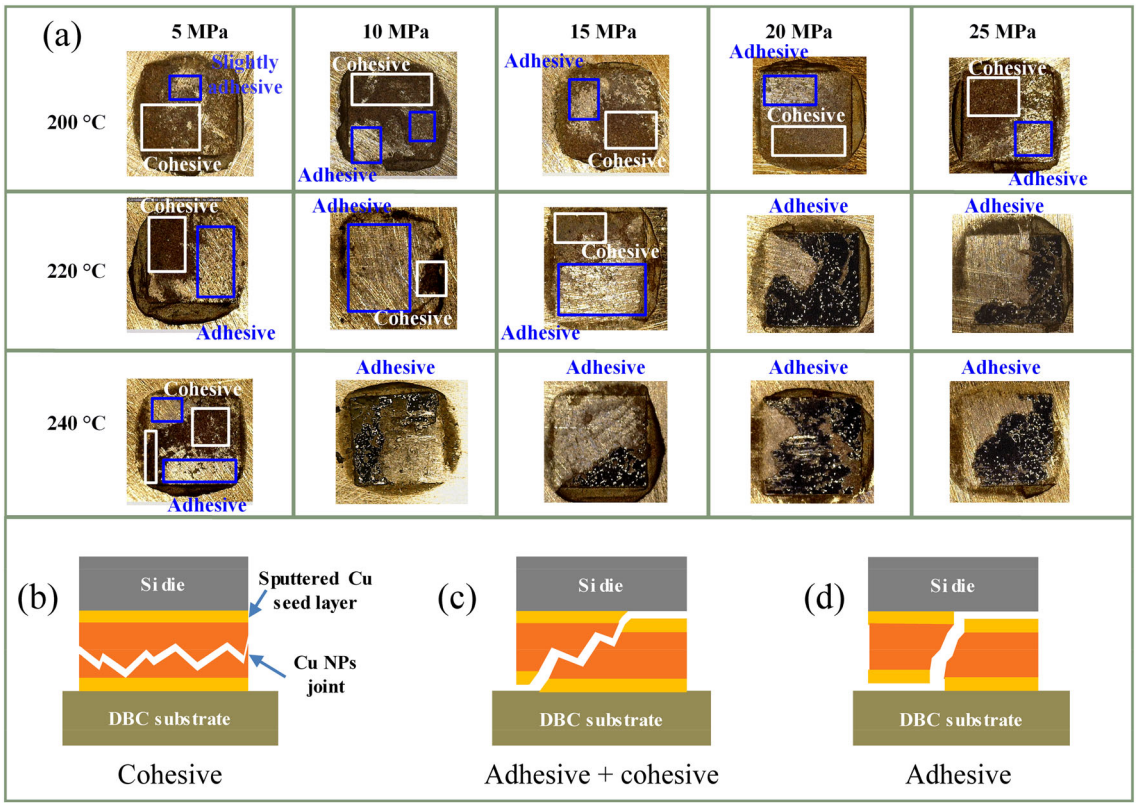

Fig. 5 **a** Sheared surfaces and fracture modes of the sintered Cu NP joints at various temperatures and pressures. Areas presenting the different fracture modes are labeled accordingly. Schematic description of the **b** cohesive, **c** mixture of adhesive and cohesive, and **d** adhesive fracture mode

on most of the fracture surfaces. The adhesive fracture (Fig. 5d) occurred primarily, at the interface between the Cu NPs and the DBC substrate. It also occurred at the interface between the sputtered Cu and Ni layers. The Cu NPs were approximately visible on the fracture surfaces. Figure 5c showed the simultaneous occurrence of the cohesive and adhesive fractures, here, the Cu joint, DBC substrate, and sputtered Cu layers were observed together. The samples that were sintering at 200 °C under different pressures presented mixed-fracture modes. The samples that were sintered at 220 °C under 5–15 MPa, also exhibited the mixed-fracture modes. However, the number of cohesive fractures was low in the samples that were subjected to pressures higher than 10 MPa. The occurrence of cohesive fractures indicated that the Cu NPs did not form strong and long-range connections. This resulted in low shear strength (Fig. 4). The Cu NPs were supplied with higher energy under high sintering pressure; consequently, they were closely compacted to form interparticle connections. This decrease the occurrence of cohesive fractures, and there was a significant increase in the shear strength with the increase in the pressure from 5 to 10 MPa at 220 °C. The fracture mode transferred from mixed to the adhesive with the increase in sintering pressure to 20 MPa and above at 220 °C. This indicated the formation of a highly condensed joint structure. The mechanical strength of the sintered joints was higher than that of the interfacial layers. The adhesive fracture mode was dominant with the increase in the sintering temperature to 240 °C, except under an external pressure of 5 MPa. The adhesive fractures occurred at two interfaces in the sample that were sintering at 240 °C under 10 MPa. This indicated the adhesive failure of the sputtered Cu seed layers and the interface before the fracture of the Cu NP joints. Consequently, the maximum increase of the shear strength was observed.

The optimal sintering temperature and pressure were determined to be 240 °C and, 10 MPa, respectively. Therefore, the samples that were sintered at 240 °C under 5, 10, and 15 MPa, were selected for the

microstructural observations (Fig. 6). When the pressure was 5 MPa (Fig. 6a–c), the fracture surface, corresponding to the cohesive model, exhibited a porous structure with Cu NPs. Figure 6b shows the region of slight plastic deformation that was introduced by the fracture. The presence of a mixture of Cu NPs was observed in this region at different sintering stages. The presence of numerous spherical particles was an indication of low-level sintering. A few Cu NPs in the center of the upper surface of the Cu joints were sintered with neck formations (Fig. 6c). The evaporated organic additives were not completely eliminated, at a low pressure of 5 MPa. Therefore, the Cu NPs were loosely packed together, and neither large sintering necks nor long-range connections were formed. This facilitated the initiation and propagation of the cracks inside the Cu joints, thereby lowering the mechanical strength.

When the sintering pressure was increased to 10 MPa (Fig. 6d), the presence of the DBC substrate, sputtered Cu layer, and a small area of the sintered Cu joint was observed in the fracture surface. The plastic deformation of the sintered NPs was initiated during failure (Fig. 6e). The formation of large sintering necks, as well as continuous connections between the neighboring Cu NPs, was observed (Fig. 6f). Therefore, the porosities of the sintered samples at 10 MPa were substantially lower than those of the sintered sample at 5 MPa. Consequently, the mechanical strengths of the sintered samples at 10 MPa were substantially higher than those of the sintered sample at 5 MPa. The decrease in the porosity of the Cu joints with the increase in the pressure from 5 to 10 MPa resulted in the removal of, most of the organic solvents in the pores. Consequently, a highly compact sintered microstructure was obtained. The crack propagation at the interfaces was easier than that inside Cu joints during the shear tests, and this results in the formation of typical adhesive fracture surfaces. The optimal sintering pressure was determined to be 10 MPa owing to the aforementioned significant changes in this condition. The sputtered Cu seed layer and DBC substrate and some area of the upper surface of the Cu NP joints

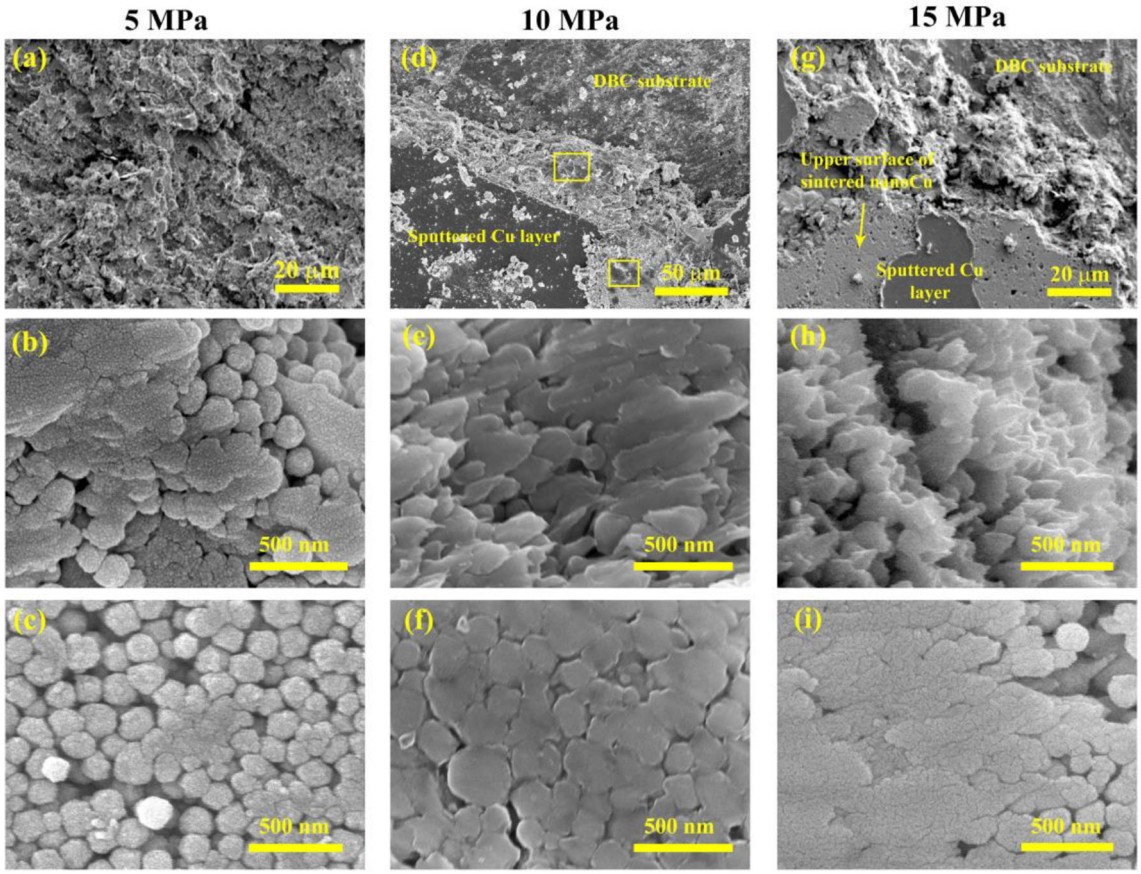

Fig. 6 SEM images of fracture surfaces of Cu NP paste sintered at 240 °C at various pressures: **a**–**c** 5 MPa, **d**–**f** 10 MPa, and **g**–**i** 15 MPa

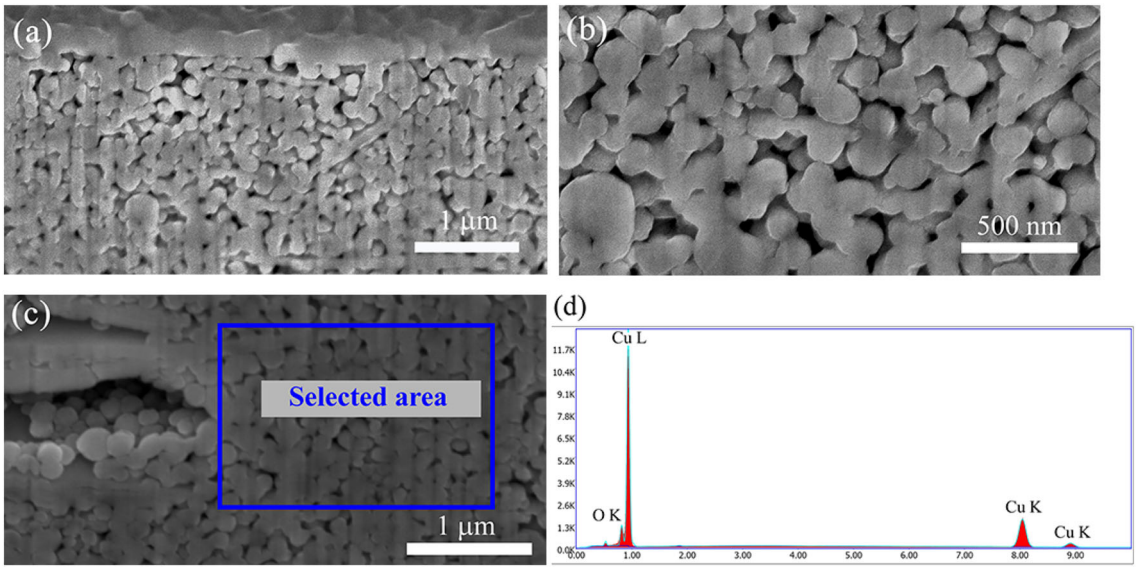

Fig. 7 **a** and **b** FIB/SEM images of the microstructure cross-section of the Cu NP joint sintered at 240 °C, 10 MPa. **c** EDX detection area on the cross-section of the Cu NP joint and **d** the spectrum

were significant observations on the adhesive fracture surface (Fig. 6g) under a sintering pressure of 15 MPa. The highly much more steep fracture surface in Fig. 6h shows the occurrence of plastic deformation. The morphology of the fracture surface at 16 MPa was similar to that of the fracture surface at 10 MPa. The integration of the Cu NPs and the low porosity of the resulting structure were indications of a high level of sintering (Fig. 6f). The vaporized organic residues between the Cu NPs were pressed out further than that at 10 MPa. The surfaces of numerous Cu NPs were exposed to surface diffusion and sintering neck formation. The condensed microstructure at a sintering pressure of 15 MPa resulted in high shear strength. There were certain similarities between not only the microstructures but also the fracture modes of the samples that were sintered under 10 and 15 MPa. However, less improvement in sintering progress was achieved from 10 to 15 MPa. Therefore, the rate of increase in shear strength was low.

Both the sintering temperature and pressure during sintering exerted an essential effect on the microstructure of the Cu NPs. The increase in the pressure resulted in the formation of a highly dense microstructure in the sintered Cu joints. This induced a substantial increase in the mechanical strength of the joints, despite the possible formation of surface oxide, due to high process temperature in air.

The cross-section microstructure of one representative sample under the optimum sintering condition (240 °C, 10 MPa), was characterized, in Fig. 7a, b. Compared to the sample processed at 240 °C, 5 MPa, more sintering neck formation between particles and lower porosity can be observed. Thus a tremendous improvement in the shear strength of this sample was obtained. Considering the possibility of oxidation at sintering temperature in air, an SEM/EDX was taken to evaluate the oxygen content within the Cu joint. As shown in Fig. 7d, a small amount of oxygen element (~ 0.5 wt%) was detected in the selected area. It could possibly have originated from two sources: surface oxidation of the Cu NPs, or organic residues from evaporation during the process. The XRD pattern of the Cu NP paste at 250 °C in the air also depicts the Cu_2O peak, which can be correlated here. Due to the small amount of oxidation, it does not have a strong negative effect on the sintering process. Condensed sintered Cu NP joints can be achieved under the appropriate sintering condition.

The increase in the sintering pressure lowers the activation energy that is required to initiate sintering, as demonstrated for the sintering of Ag NP paste [33]. Since Cu and Ag may possess similar metallic properties, the increase in the sintering pressure possibly decreases the activation energy for the sintering of Cu NPs. Figure 8 shows a schematic elaboration of the effect of the pressure during in-air sintering. Prior to the sintering, the Cu NPs in the paste were separated

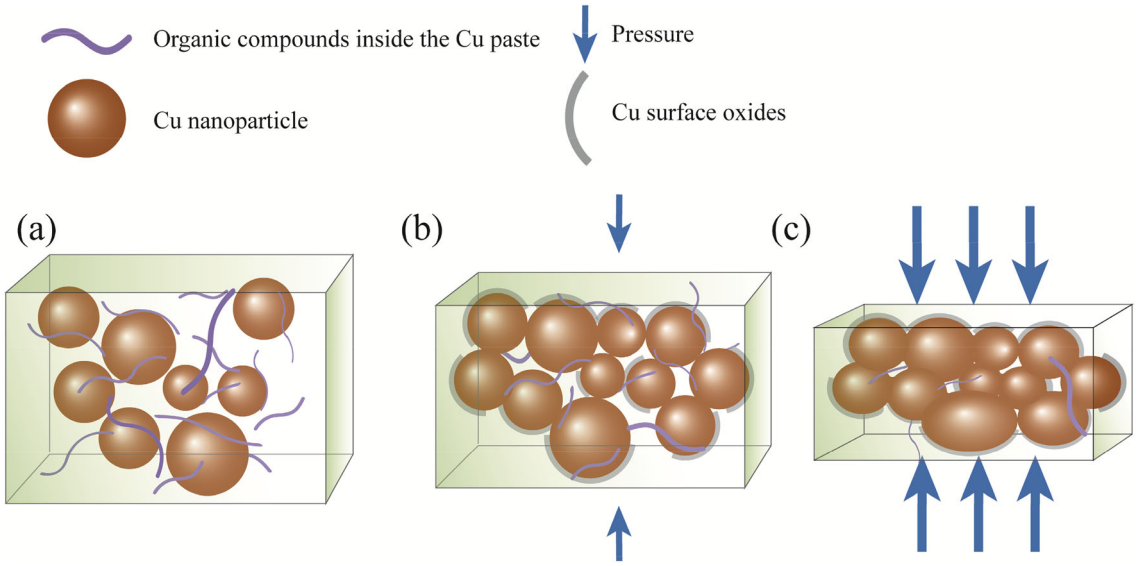

Fig. 8 Schematic of the effect of the pressure during sintering of the Cu NP paste. **a** Cu NP paste before sintering. **b** Cu NP paste that is sintered under low pressure and **c** high pressure

by complex organic additives, and the particle surfaces are covered to prevent oxidation and sintering. The vaporized organic additives and the air are partially removed with the assistance of low pressure, thereby resulting in the exposure of the Cu NP surfaces. This facilitated the diffusion of Cu atoms between the particles, which induced the formation of sintering necks [33–36]. Since the sintering was performed at a relatively high temperature in air, the surfaces of the Cu NPs underwent slight oxidation. The presence of the organic residue induced the formation of the voids, furthermore, possible oxidation increased the distance between the particles. This prevented the formation of long-range and continuous connections under low pressure, thereby decreasing the mechanical strength. Most of the evaporated organic additives and air were eliminated with the increase in the sintering pressure. This resulted in the exposure of approximately all the Cu NP surfaces and the subsequent close packing of the particles. Thus, sintering was initiated. The presence of a low volume of air during sintering also prevented the occurrence of additional oxidation at the process temperatures. Advanced levels of sintering, which resulted in the formation of condensed microstructures and 3D connection, was achieved under high pressure. This resulted in a significant increase in the shear strength of the sintered joints, even without protective atmosphere. It was concluded that the low-temperature sintered Cu NP paste could be utilized for the die attach in power electronics applications.

4 Conclusion

The in-air sintering behavior of a Cu NP paste under various process conditions was investigated in this study. The in-air sintering temperature range was determined based on the results of the characterization of the paste and multiple pressure-assisted sintering experiments were performed in air. Highly condensed structures with close-packed Cu NPs were formed with the increase in the sintering temperature and pressure. The increase in the sintering temperature and pressure accelerate the formation of sintering necks and interparticle connections inside the Cu joints. A maximum shear strength of 41.63 ± 4.35 MPa was obtained at the sintering temperature, pressure, and time of 240 °C, 25 MPa, and 3 min, respectively. Furthermore, the highest increase in the shear strength was observed for the samples that were sintered at 240 °C under 10 MPa. These samples presented a high shear strength of 28.1 ± 8.47 MPa, which satisfied the requirements for die attach in power electronics applications. The optimal sintering condition was determined to be 240 °C and 10 MPa, because the cost of production and the risk of damage to the die are high at high pressures. The experimental and characterization

results revealed that a Cu NP paste that is subjected to in-air sintering with pressure assistance can be utilized for die-attach in power electronics applications.

Acknowledgements

This work received support from the XRD Facility of the Mechanical, Maritime and Materials Engineering (3mE) Faculty of the Delft University of Technology.

Author contributions

BZ wrote the main manuscript. BZ, AD, and JZ performed the sintering experiments together. AD, JZ, HZ, YZ, JF, and GZ reviewed the manuscript.

Funding

This research was carried out under Project Number T16017 within the Framework of the Research Program of the Materials Innovation Institute (M2i) (www.m2i.nl) supported by the Dutch government. This work was partially supported by the National Natural Science Foundation of China (61704033).

Compliance with ethical standards

Conflict of interest The authors declare no competing interest.

References

1. H.A. Mantooth, M.D. Glover, P. Shepherd, Wide bandgap technologies and their implications on miniaturizing power electronic systems. IEEE J. Emerg. Sel. Top. Power Electron. **2**, 374–385 (2014). https://doi.org/10.1109/JESTPE.2014.2313511
2. P.G. Neudeck, R.S. Okojie, L. Chen, High-temperature electronics—a role for wide bandgap semiconductors? Proc. IEEE **90**, 1065–1076 (2002). https://doi.org/10.1109/JPROC.2002.1021571
3. W. Arden, et al., *More-than-Moore White Paper*, ITRS White Paper 14 (2010)
4. T. Siewert, *Properties of Lead-Free Solders* (Colorado School of Mines, Golden, 2002).
5. K.S. Siow, *Die-Attach Materials for High Temperature Applications in Microelectronics Packaging* (Springer, Cham, 2019).
6. W. Chen, W. Bottoms, K. Pressel, J. Wolf, *The Next Step in Assembly and Packaging: System Level Integration in the Package (SiP)*, ITRS White Paper 9 (2008)
7. D. Lu, C.P. Wong, *Materials for Advanced Packaging*, vol. 181 (Springer, New York, 2009).
8. P. Buffat, J.P. Borel, Size effect on the melting temperature of gold particles. Phys. Rev. A **13**, 2287–2298 (1976). https://doi.org/10.1103/PhysRevA.13.2287
9. K.N. Tu, Reliability challenges in 3D IC packaging technology. Microelectron. Reliab. **51**, 517–523 (2011). https://doi.org/10.1016/j.microrel.2010.09.031
10. M.Y. Xiong, L. Zhang, Interface reaction and intermetallic compound growth behavior of Sn–Ag–Cu lead-free solder joints on different substrates in electronic packaging. J. Mater. Sci. **54**, 1741–1768 (2019). https://doi.org/10.1007/s10853-018-2907-y
11. Z. Zhang et al., Low-temperature and pressureless sinter joining of Cu with micron/submicron Ag particle paste in air. J. Alloys Compd. **780**, 435–442 (2019). https://doi.org/10.1016/j.jallcom.2018.11.251
12. S.S. Kim, Mechanical properties of nano-silver joints as die attach materials. J. Alloys Compd. **514**, 6–19 (2012). https://doi.org/10.1016/j.jallcom.2011.10.092
13. J.T. Jiu et al., Die-attaching silver paste based on a novel solvent for high-power semiconductor devices. J. Mater. Sci. **51**, 3422–3430 (2016). https://doi.org/10.1007/s10853-015-9659-8
14. C. Du, X. Li, Y. Mei, G. Lu, An explanation of sintered silver bonding formation on bare copper substrate in air. Appl. Surf. Sci. **490**, 403–410 (2019). https://doi.org/10.1016/j.apsusc.2019.06.105
15. H. Zhang et al., Effects of sintering pressure on the densification and mechanical properties of nanosilver soluble-side sintered power module. IEEE Trans. Compon. Packag. Manuf. Technol. **9**, 963–972 (2019). https://doi.org/10.1109/tcpmt.2018.2884032
16. J. Wu, C.C. Lee, Low-pressure solid-state bonding technology using fine-grained silver foils for high-temperature electronics. J. Mater. Sci. **53**, 2618–2630 (2018). https://doi.org/10.1007/s10853-017-1689-y
17. J. Li, C.M. Johnson, C. Buttay, W. Sabbah, S. Azzopardi, Bonding strength of multiple SiC die attachment prepared by sintering of Ag nanoparticles. J. Mater. Process. Technol. **215**, 299–308 (2015). https://doi.org/10.1016/j.jmatprotec.2014.08.002
18. C. Chen et al., Necking growth and mechanical properties of sintered Ag particles with different shapes under air and N_2

atmosphere. J. Mater. Sci. **54**, 13344–13357 (2019). https://doi.org/10.1007/s10853-019-03813-0

19. C.T. Chen et al., Low temperature low pressure solid-state porous Ag bonding for large area and its high-reliability design in die-attached power modules. Ceram. Int. **45**, 9573–9579 (2019). https://doi.org/10.1016/j.ceramint.2018.10.046
20. R. Riva, C. Buttay, B. Allard, P. Bevilacqua, Migration issues in sintered-silver die attaches operating at high temperature. Microelectron. Reliab. **53**, 1592–1596 (2013). https://doi.org/10.1016/j.microrel.2013.07.103
21. H. Zhang et al., Microstructural and mechanical evolution of silver sintering die attach for SiC power devices during high temperature applications. J. Alloys Compd. **774**, 487–494 (2019). https://doi.org/10.1016/j.jallcom.2018.10.067
22. M. Yeadon, J.C. Yang, R.S. Averback, In situ observations of classical grain growth mechanisms during sintering of copper nanoparticles on (001) copper. Appl. Phys. Lett. **71**, 1631–1633 (1997). https://doi.org/10.1063/1.120000
23. J. Liu, H. Chen, H. Ji, M. Li, Highly conductive Cu–Cu joint formation by low-temperature sintering of formic acid-treated Cu nanoparticles. ACS Appl. Mater. Interfaces **8**, 33289–33298 (2016). https://doi.org/10.1021/acsami.6b10280
24. H. van Zeijl, W. et al., in *The 66th Electronic Components and Technology Conference (ECTC)* (IEEE, 2016), pp. 217–224
25. B. Zhang et al., in *The 17th International Conference of Electronic Packaging Technology (ICEPT)* (IEEE, 2016), pp. 1163–1167
26. J. Li et al., Low-temperature and low-pressure Cu–Cu bonding by highly sinterable Cu nanoparticle paste. Nanoscale Res. Lett. **12**, 255 (2017). https://doi.org/10.1186/s11671-017-2037-5
27. H. Nakako et al., in *International Exhibition and Conference for Power Electronics, Intelligent Motion, Renewable Energy and Energy Management (PCIM Europe 2017)* (VDE, 2017), pp. 1–5
28. H. Nakako, et al., in *International Exhibition and Conference for Power Electronics, Intelligent Motion, Renewable Energy and Energy Management (PCIM Europe 2018)* (VDE, 2018), pp. 1–6
29. Y. Zuo, J. Shen, Y. Hu, R. Gao, Improvement of oxidation resistance and bonding strength of Cu nanoparticles solder joints of Cu–Cu bonding by phosphating the nanoparticle. J. Mater. Process. Technol. **253**, 27–33 (2018). https://doi.org/10.1016/j.jmatprotec.2017.11.001
30. Y.Y. Dai et al., Enhanced copper micro/nano-particle mixed paste sintered at low temperature for 3D interconnects. Appl. Phys. Lett. **108**, 263103 (2016). https://doi.org/10.1063/1.4954966
31. K.H. Jung, K.D. Min, C.J. Lee, S.B. Jung, Pressureless die attach by transient liquid phase sintering of Cu nanoparticles and Sn–58Bi particles assisted by polyvinylpyrrolidone dispersant. J. Alloys Compd. **781**, 657–663 (2019). https://doi.org/10.1016/j.jallcom.2018.12.032
32. Y. Zuo, J. Shen, J. Xie, L. Xiang, Influence of Cu micro/nano-particles mixture and surface roughness on the shear strength of Cu–Cu joints. J. Mater. Process. Technol. **257**, 250–256 (2018). https://doi.org/10.1016/j.jmatprotec.2018.03.005
33. P. Peng et al., Joining of silver nanomaterials at low temperatures: processes, properties, and applications. ACS Appl. Mater. Interfaces **7**, 12597–12618 (2015). https://doi.org/10.1021/acsami.5b02134
34. J.W. Yoon, J.H. Back, Effect of sintering conditions on the mechanical strength of Cu-sintered joints for high-power applications. Materials **11**, 2105–2117 (2018). https://doi.org/10.3390/ma11112105
35. Y. Seong et al., Dominant mechanisms of the sintering of copper nano-powders depending on the crystal misalignment. Comput. Mater. Sci. **123**, 164–175 (2016). https://doi.org/10.1016/j.commatsci.2016.06.016
36. Y. Zhang, L. Wu, X. Guo, Y.-G. Jung, J. Zhang, Molecular dynamics simulation of electrical resistivity in sintering process of nanoparticle silver inks. Comput. Mater. Sci. **125**, 105–109 (2016). https://doi.org/10.1016/j.commatsci.2016.08.047